ORIGINAL PAPER

Synthesis and electrochemical properties of a cubic polymorph of LiNi$_{1/2}$Mn$_{1/2}$O$_2$ with a spinel framework

Kingo Ariyoshi[1] · Kensuke Kajikawa[1] · Yusuke Yamada[1]

Abstract

Employment of high-capacity positive-electrode materials is one of the most effective ways to improve the energy density of Li-ion batteries. The electrochemical properties of Li transition-metal oxides, which make up the Li insertion materials in the positive electrode, depend on their crystal structures. In general, materials composed of LiMO$_2$ (M: a transition metal) with a layered structure (i.e., a two-dimensional framework) exhibit a high capacity, but complete extraction of the Li ions in the framework results in destruction of the structure. LiM$_2$O$_4$ having a spinel structure (i.e., a three-dimensional framework) exhibits excellent toughness, but the number of Li ions in the structure is smaller than that in the layered structure, resulting in a lower reversible capacity. Li$_2$M$_2$O$_4$ with a reduced spinel-framework structure can be expected to have the advantages of both layered and spinel structures: high capacity and robust structure. In this study, a cubic polymorph of LiNi$_{1/2}$Mn$_{1/2}$O$_2$, which is thought to be a layered material, was prepared by low-temperature synthesis. The obtained LiNi$_{1/2}$Mn$_{1/2}$O$_2$ was electrochemically active and showed a reversible capacity of > 100 mAh g^{-1} at an upper limit voltage of 4.2 V, which is almost the same as that of a two-dimensional material with a layered structure. To confirm the crystal structure of low-temperature LiNi$_{1/2}$Mn$_{1/2}$O$_2$, the change in crystal structure during Li extraction was investigated by ex situ XRD measurements. The isotropic contraction of the cubic lattice during Li extraction causes low-temperature LiNi$_{1/2}$Mn$_{1/2}$O$_2$ to have a cubic lattice rather than a layered structure with a pseudo-cubic lattice. The crystal structure of low-temperature LiNi$_{1/2}$Mn$_{1/2}$O$_2$ with a cubic lattice and the Li extraction mechanism were elucidated from these results.

Keywords Lithium-ion battery · Lithium nickel manganese oxide · Reduced spinel · Low-temperature synthesis

Introduction

Li-ion batteries, which are used to power electric vehicles, are a key technology in achieving a sustainable, low-carbon society [1–4]. Developing novel electrode materials is the most effective way of improving battery performance. The Li insertion materials commonly used as both positive and negative electrodes undergo topotactic lithium insertion/extraction reactions during charge and discharge processes. Li ions are reversibly inserted into or extracted from the crystal lattice with maintaining the framework constructed of transition metal(s) and oxygen [5–8]. Such materials typically possess layered, spinel, forsterite (olivine), or rutile crystal structures [9–14]. All of these have vacant sites for the accommodation of Li ions and Li-ion conducting pathways both of which are two necessary features for Li insertion/extraction.

The electrochemical properties of lithium insertion materials, such as the electrode potential and reversible capacity, are highly dependent on the crystal structure. For example, layered materials typified by LiMO$_2$ (M: a transition metal) are described as having high capacities because the crystal lattice contains a large number of lithium ions. However, owing to its two-dimensional framework, extraction of most of the Li ions leads to structural collapse and loss of reversibility [15–18]. Therefore, it is not possible to fully utilize the theoretical capacity of layered materials. By contrast, materials with a spinel structure are capable of complete Li-ion extraction because they have a robust, three-dimensional framework, resulting in a reversible capacity that is close to the theoretical value [19–22]. The high structural stability of these materials offers excellent cyclability [23–25]. However,

✉ Kingo Ariyoshi
  ariyoshi@osaka-cu.ac.jp

1 Department of Applied Chemistry and Bioengineering, Graduate School of Engineering, Osaka City University, 3-3-138 Sugimoto, Sumiyoshi, Osaka 558-8585, Japan

the theoretical capacity for spinel materials with a chemical composition of LiM_2O_4 is small because the amount of Li extraction/insertion is half that of layered-structure materials.

Previous studies have reported that $LiCoO_2$ calcined at low temperature (LT-$LiCoO_2$) has a spinel framework, although the composition is the same as layered-structure materials (i.e., $LiMO_2$) [26–33]. LT-$LiCoO_2$ obtained by low-temperature synthesis is a polymorph of the high-temperature phase of $LiCoO_2$, which has a layered structure [29, 34, 35]. LT-$LiCoO_2$ adopts a reduced (or lithiated) spinel structure, meaning that it has the structure of a spinel material that has undergone reduction, $LiM_2O_4 + Li^+ + e^- \rightleftarrows Li_2M_2O_4$. Owing to the composition and three-dimensional structure, LT-$LiCoO_2$ is expected to have the advantages of both the layered and spinel structures (i.e., a large reversible capacity with excellent reversibility).

In this study, to further develop a series of materials with reduced spinel structures, $LiNi_{1/2}Mn_{1/2}O_2$ (LNMO), which has a layered structure when prepared via high-temperature synthesis [36–40], was prepared via low-temperature synthesis to obtain the polymorphic reduced spinel structure. The crystal structure of the synthesized material was identified by examining the changes in the crystal structure during Li extraction. The potential to employ this material as a high-capacity positive-electrode material was examined with regards to the Li-insertion mechanism.

Experimental methods

Synthesis of lithium nickel manganese oxides LNMOs were prepared at various temperatures (450–1000 °C) by heating a reaction mixture of Li_2CO_3 and nickel manganese double hydroxide (Ni: Mn = 0.994:1.006; Tanaka Chemical Co., Japan) with the molar ratio of Li:(Ni + Mn) = 1:1 for 16 h in air. The synthesized materials were characterized by powdered XRD using an X-ray diffractometer (XRD-6100, Shimadzu Corp., Japan) equipped with a graphite monochromator using Fe Kα radiation operated at 40 kV and 15 mA. Data were collected over a 2θ range of 10 to 100° at a scan rate of 0.5° min^{-1}. The change in the crystal structure of the materials during Li extraction was also characterized by ex situ XRD. Ex situ XRD patterns were obtained from an electrode taken out from a cell and covered with polyethylene film to avoid any reaction with moisture. Thermogravimetric analysis was performed using a TG analyzer (TGA-60 Plus, Shimadzu Corp., Japan). The sample (~ 10 mg) was placed into a platinum dish and heated to 1000 °C at a constant rate of 5 °C min^{-1} in air.

Electrochemical measurements of lithium nickel manganese oxides An electrochemical cell that can be used for LNMO material testing has been reported previously [31]. To prepare the positive electrode, a black viscous slurry consisting of 88 wt% active materials, 6 wt% acetylene black, and 6 wt% polyvinylidene fluoride dispersed in N-methyl-2-pyrrolidone was cast onto aluminum foil. The electrode was dried under vacuum at 150 °C overnight to evaporate N-methyl-2-pyrrolidone. Finally, the electrode was punched out to form a disk (16.0 mm diameter). The loading weight of the electrode mix was approximately 15 mg cm^{-2}. A Li metal electrode was used as the negative electrode. A 1 M solution of $LiPF_6$ in 3:7 (v/v) ethylene carbonate/dimethyl carbonate (Kishida Chemical Co., Ltd., Japan) was used as the electrolyte. Electrochemical testing was carried out using a battery cycler (Battery Laboratory System, Keisokuki Center Co., Ltd., Japan).

Results

Crystal structure and electrochemical behavior of low-temperature lithium nickel manganese oxide No significant weight loss was observed in the thermogravimetric curve above 500 °C (Figure S1), indicating that the chemical composition of LNMO calcined above 500 °C was identical to that of $LiNi_{1/2}Mn_{1/2}O_2$. The XRD patterns of LNMO calcined at various temperatures are given in Fig. 1. No diffraction peak derived from the raw material powder was observed in the XRD patterns of the samples calcined at any temperature, indicating that all reactions proceeded completely. As the calcination temperature was increased, the diffraction peaks became sharper and splitting of the peak at 84° became more defined. For the samples calcined at 900 °C and 1000 °C, a clear split of this peak into (108) and (110) peaks was observed, and so it was deduced that the structure was one in which alternating layers of lithium and the transition-metal are stacked. As such, the diffraction pattern was indexed as a hexagonal lattice. Meanwhile, for the samples calcined at temperatures below 750 °C, it could not be determined whether the lattice symmetry was hexagonal or cubic. The diffraction peak located at 84° can be used to identify the lattice symmetry: for a hexagonal lattice, the peak should be split into two ((108) and (110) peaks), whereas for a cubic lattice, a single (440) peak should be observed. However, the broadness of the peak disturbed to distinguish whether it is actually a single peak or if it is rather two overlapping peaks.

Figure 2a shows the lattice parameters of the samples, calculated by the least squares method using the Miller indices and diffraction angles. Hexagonal lattice parameters were calculated to compare the parameters of each sample on the same basis because the symmetry of the hexagonal lattice is lower than that of the cubic lattice. We used 7–10 peaks to calculate the lattice parameters, whose standard deviations did not exceed ± 0.2% and ± 0.03% at most for LNMO calcined at low and high temperatures, respectively. The lattice constant was found to continuously change with respect to the calcination temperature; as the calcination temperature increased, the c_h-axis increased while the a_h-axis remained constant.

Fig. 1 XRD patterns of LiNi$_{1/2}$Mn$_{1/2}$O$_2$ synthesized at **a** 1000 °C, **b** 900 °C, **c** 750 °C, **d** 600 °C, and **e** 500 °C in air for 16 h
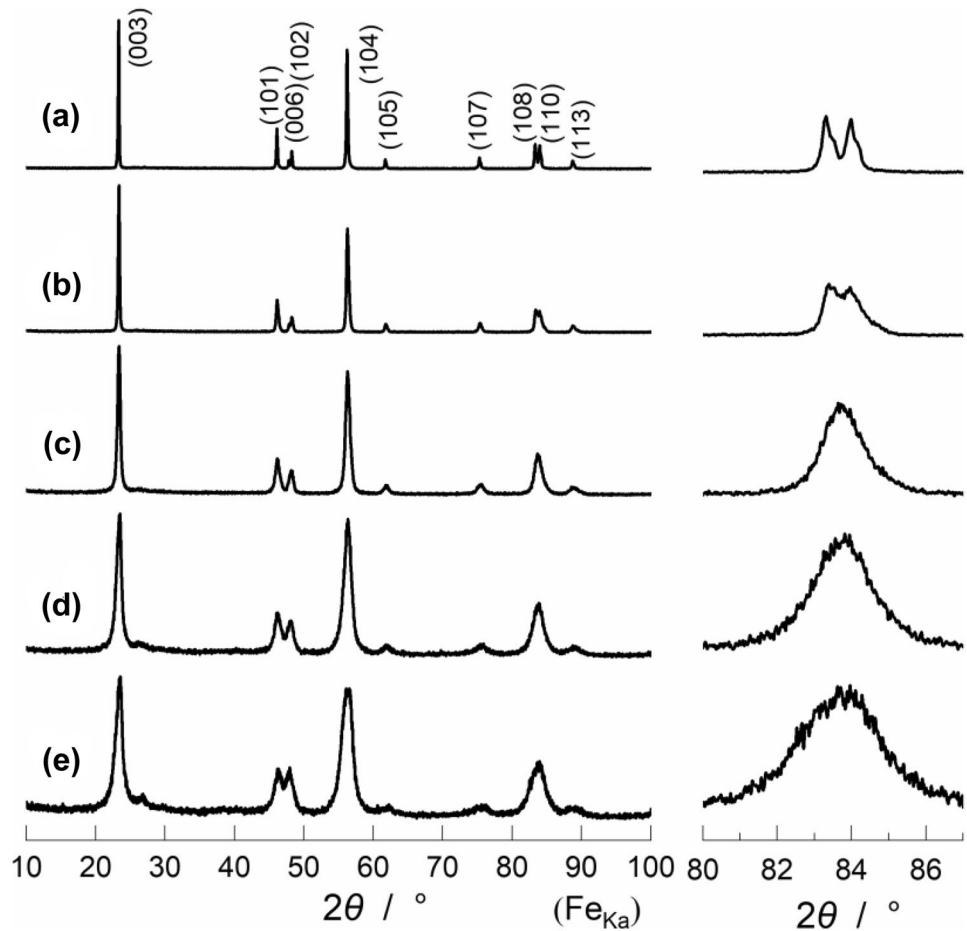
Consequently, the lattice volume increased with increasing calcination temperature. To investigate whether the crystal lattice is cubic, the value of c_h/a_h was calculated and is plotted in Fig. 2b. The cubic lattice parameter a_c can be used to calculate a_h and c_h of the layered structure using the following equation:

$$a_h = a_c/2\sqrt{2} \text{ and } c_h = a_c \times \sqrt{3} \tag{1}$$

From Eq. (1), a cubic lattice gives a c_h/a_h value of 4.9 [41, 42]. As can be seen in Fig. 2b, the c_h/a_h values for samples calcined below 550 °C were approximately 4.9 and increased
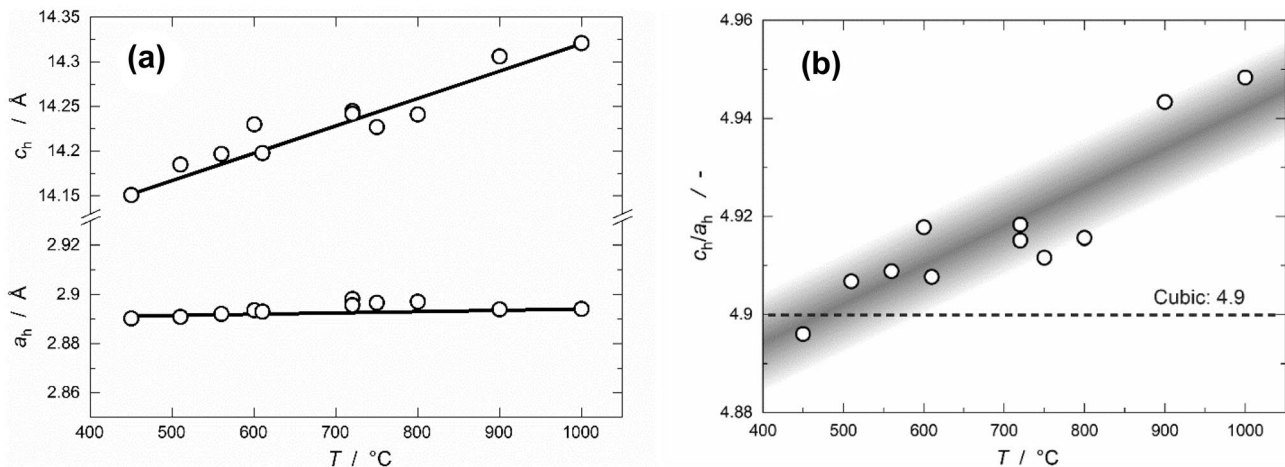

Fig. 2 **a** Hexagonal lattice parameters of LiNi$_{1/2}$Mn$_{1/2}$O$_2$ calcined at various temperatures. **b** c_h/a_h versus calcination temperature for LiNi$_{1/2}$Mn$_{1/2}$O$_2$ samples

Fig. 3 Charge–discharge curves of Li/LiNi$_{1/2}$Mn$_{1/2}$O$_2$ cells operated at 0.25 mA cm^{-2} in the voltage range of 2.5–4.2 V for 5 cycles. Positive electrodes were LiNi$_{1/2}$Mn$_{1/2}$O$_2$ calcined at **a** 900 °C, **b** 750 °C, **c** 600 °C, and **d** 500 °C. Blue lines indicate charge and discharge curves for the initial cycle
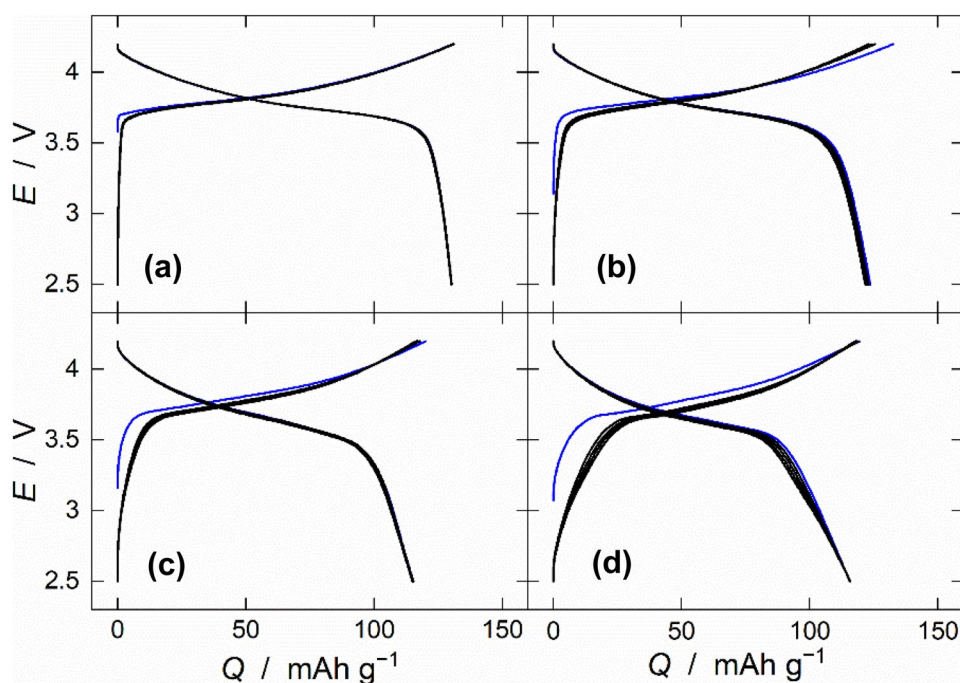

with increasing calcination temperature. This suggests that LNMO has a cubic lattice when prepared at low temperature and a hexagonal lattice when prepared at high temperature.

To examine the electrochemical properties of LT-LNMO, constant-current charge–discharge tests were performed (Fig. 3). A reversible capacity of > 100 mAh g^{-1} was measured for all samples at an operating voltage of 2.5 to 4.2 V. The shapes of the charge–discharge curves became gentler for low

calcination temperatures. The changes in the voltage profiles (operating voltage and voltage shape) of LNMO are not as significant as those of LiCoO$_2$, for which the curve shape changes drastically as the structure changes from layered to spinel. Differential chronopotentiograms (dQ/dE plots) were obtained to investigate the solid-state redox potential of LNMO (Fig. 4). The electrode potential was found to decrease with decreasing calcination temperature. While layered LNMO samples (i.e.,

Fig. 4 Differential chronopotentiograms calculated from charge/discharge curves. The positive electrodes used were LiNi$_{1/2}$Mn$_{1/2}$O$_2$ calcined at **a** 900 °C, **b** 750 °C, **c** 600 °C, and **d** 500 °C
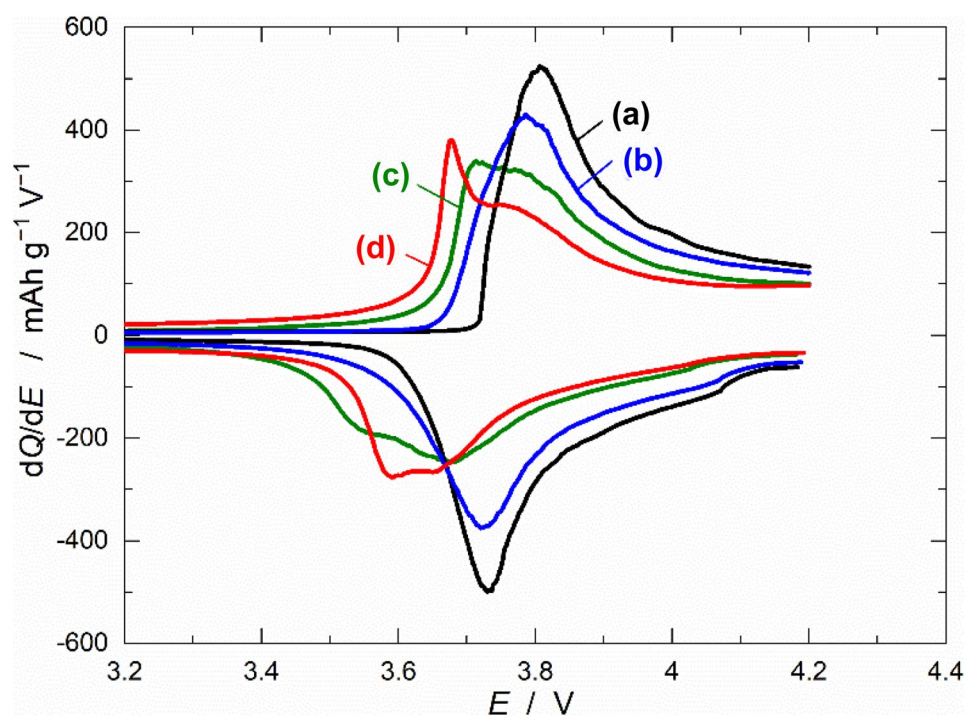
those calcined at > 900 °C) showed an oxidation peak at 3.81 V and a reduction peak at 3.73 V, samples with a cubic symmetry showed oxidation and reduction peaks at ~ 3.7 V and ~ 3.6 V, respectively. This indicates that the solid-state redox potential of LT-LNMO is lower than that of the high-temperature phase, a behavior which is similar to that of $LiCoO_2$ [29–31].

Lattice parameter changes in low-temperature $LiNi_{1/2}Mn_{1/2}O_2$ during Li extraction Although the crystal lattice of LT-LNMO (calcined at 500 °C) has a cubic symmetry, it may actually have a layered structure with a pseudo-cubic lattice. Its crystal structure cannot be identified from a structural refinement using the Rietveld method owing to the broad diffraction peaks observed and the fact that diffraction peaks of layered and spinel structures have the same relative intensities (Table S1). To identify whether the crystal lattice is cubic or hexagonal with pseudo-cubic lattice parameters, the change in the lattice parameters of LNMO during Li extraction was investigated. Materials with a hexagonal lattice typified by a layered structure exhibit anisotropic change in the crystal lattice during Li extraction (i.e., a_h-axis shrinkage and c_h-axis expansion) [40]. Materials with a cubic lattice typified by a spinel framework, however, exhibit isotropic change during extraction (i.e., a_c-axis shrinkage)

[19, 21, 22]. Therefore, to identify the crystal symmetry of LT-LNMO, ex situ XRD measurements were performed.

Figure 5 shows the XRD patterns of LNMO calcined at 500 °C charged to various capacities. The diffraction peaks continuously shift toward higher diffraction angles. The diffraction patterns remained the same regardless of the state of charge. In particular, the shape of the diffraction peak at 84° remained unchanged (i.e., no splitting was observed) and the peak width remained almost constant. This suggests that upon Li extraction, the cubic lattice of LT-LNMO is maintained. To confirm the crystal symmetry of LT-LNMO, the hexagonal lattice parameters of the charged materials were calculated (Fig. 6). The lattice parameters of layered LNMO obtained by high-temperature synthesis (900 °C) are also shown in the figure for comparison. The high- and low-temperature phases of LNMO exhibited different behaviors with respect to the change in lattice parameters during lithium extraction. The lattice parameters of layered LNMO exhibited anisotropic change: expansion of the c_h-axis and shrinkage of the a_h-axis, resulting in the c_h/a_h value increasing to 5.1 during Li extraction. This anisotropic change is generally observed in lithium insertion materials, which have layered structure [40]. In contrast to the anisotropic

Fig. 5 XRD patterns of **a** pristine $LiNi_{1/2}Mn_{1/2}O_2$ calcined at 500 °C and $LiNi_{1/2}Mn_{1/2}O_2$ electrodes with charged capacities of **b** 31 mAh g⁻¹, **c** 63 mAh g⁻¹, and **d** 113 mAh g⁻¹. Peaks denoted PE arise from the polyethylene film
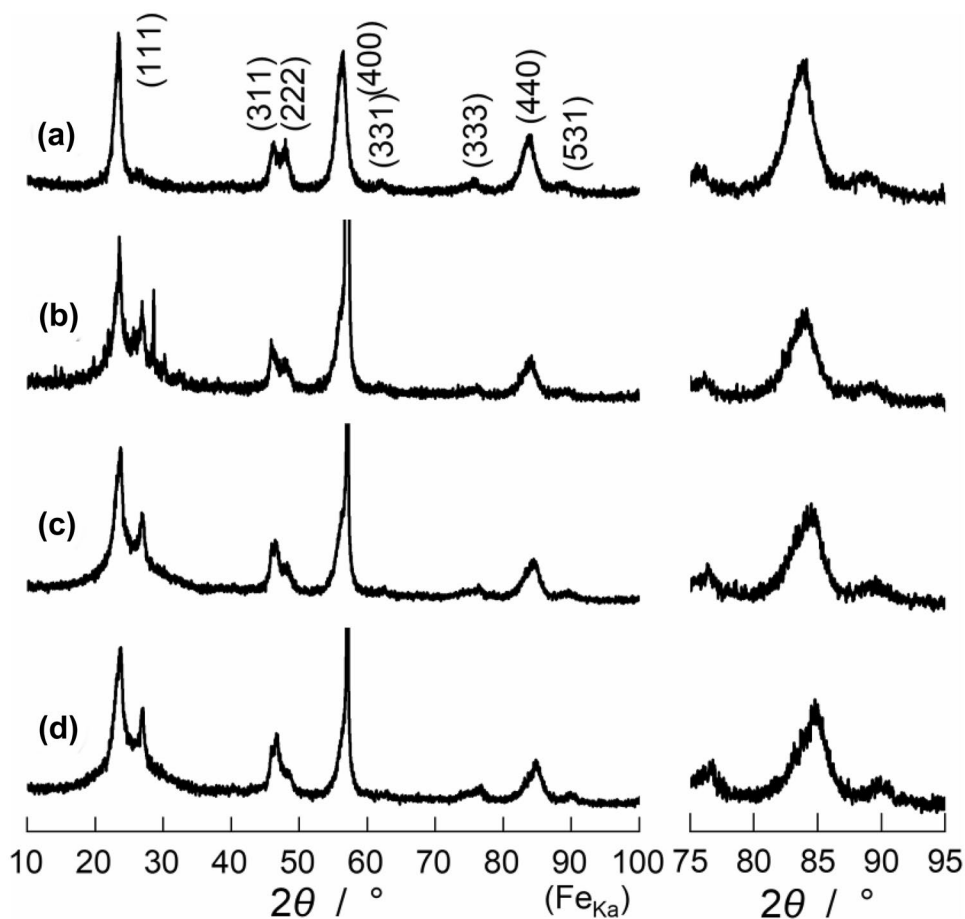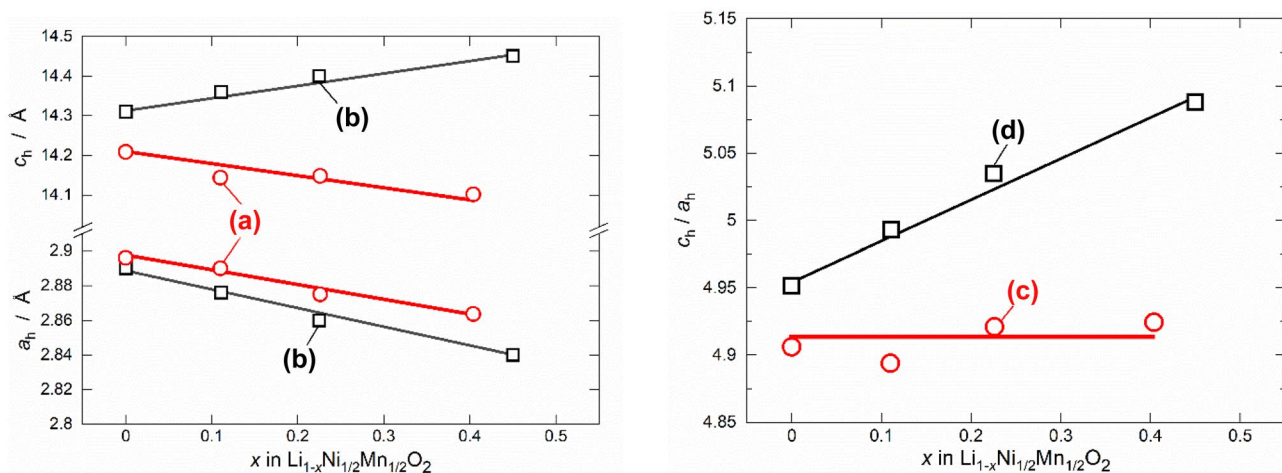
Fig. 6 Hexagonal lattice parameters of $Li_{1-x}Ni_{1/2}Mn_{1/2}O_2$ calcined at **a** 500 °C and **b** 900 °C during Li extraction. The ratio of hexagonal lattice parameters, c_h/a_h, of $LiNi_{1/2}Mn_{1/2}O_2$ calcined at **c** 500 °C and **d** 900 °C

change in the high-temperature phase, the crystal lattice of LT-LNMO was found to change isotropically: a shrinkage in both the a_h- and c_h-axes was observed. The value of c_h/a_h remained constant at approximately 4.9 during Li extraction, indicating that the crystal lattice of the low-temperature phase has cubic symmetry.

Because LT-LNMO has cubic symmetry, all the diffraction peaks in Fig. 5 were assigned Miller indices with the cubic lattice, and the cubic-lattice constant was calculated using 6–8 peaks (Fig. 7). The standard deviation of the cubic-lattice parameter is $\pm 0.1\%$ (± 0.01 Å), which is

relatively small compared to the change in the lattice constant. The lattice constant of $Li_{1-x}Ni_{1/2}Mn_{1/2}O_2$ changed linearly as a function of x. Li extraction was found to proceed as a homogeneous-phase reaction for $LiNi_{1/2}Mn_{1/2}O_2$ because the lattice constant changed continuously. When 0.4 mol of Li ions was extracted from $LiNi_{1/2}Mn_{1/2}O_2$, the cubic lattice parameter decreased to 8.11 Å as $Li_{0.6}Ni_{1/2}Mn_{1/2}O_2$ was formed (i.e., a 3% shrinkage of the lattice volume). This is a smaller volume shrinkage than other spinel materials exhibit; $Li[Ni_{1/2}Mn_{3/2}]O_4$ decreases by 4.9% and $LiMn_2O_4$ by 5.3% [19, 43]. This cannot be explained based on the

Fig. 7 Cubic lattice parameters of $Li_{1-x}Ni_{1/2}Mn_{1/2}O_2$
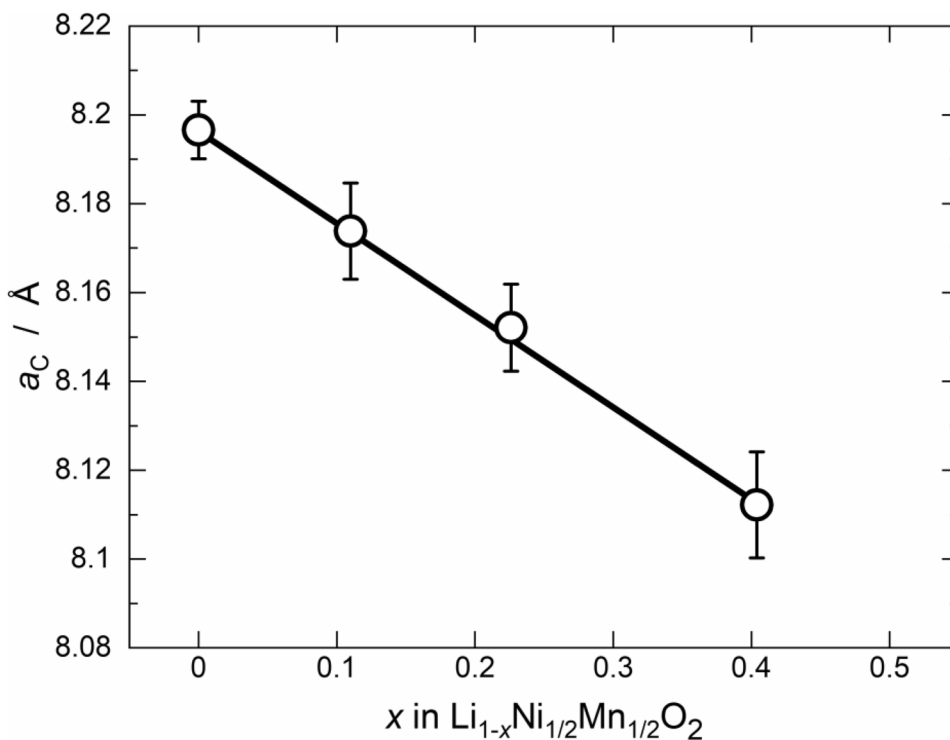
change in the ionic radius of the redox species (0.115 Å for Mn^{3+} (high spin)/Mn^{4+} versus 0.13 Å for Ni^{2+}/Ni^{3+} (low spin)) even though the dimensional changes of lithium insertion materials, which have a spinel structure exhibit, are related to the ionic radius [44]. The reason for the difference in volume shrinkage may be due to the change in crystal lattice symmetry,a cubic lattice is distorted to a tetragonal lattice for $Li[Ni_{1/2}Mn_{3/2}]O_4$ and $LiMn_2O_4$, while a cubic lattice is maintained for $LiNi_{1/2}Mn_{1/2}O_2$.

Charging $LiNi_{1/2}Mn_{1/2}O_2$ electrodes to 5 V To examine whether all the Li ions can be extracted from LT-LNMO, a $Li/LiNi_{1/2}Mn_{1/2}O_2$ cell was charged up to 4.9 V (Fig. 8). The initial charging capacity was approximately 280 mAh g^{-1}, which was the theoretical capacity based on the assumption that all Li ions in the structure were extracted. However, the discharge capacity was only 180 mAh g^{-1}, which is significantly lower than the charge capacity. The amount of inserted Li ions was calculated from the discharge capacity to be approximately 0.65, suggesting that more than half of the available Li can be inserted into $LiNi_{1/2}Mn_{1/2}O_2$, but the material does not return to the initial state upon discharging. In the differential chronopotentiogram calculated from the charge–discharge curves (Figure S2), oxidation peaks arising from Li extractions were observed at 3.7, 3.8, and 4.45 V, and reduction peaks arising from Li insertion were observed at 3.4 V and 3.6 V. These paired peaks (3.7 V/3.4 V and 3.8 V/3.6 V) indicate that lithium extraction/insertion reactions proceed reversibly in this voltage region. However, at voltages above 4.3 V, the lithium insertion reaction is not reversible, and only a peak for the oxidation reaction was observed. By observation of the charge–discharge curves alone, it is difficult to say whether the reaction above 4.3 V is lithium extraction.

To ascertain whether all Li ions can be extracted from LT-LNMO, XRD analysis was carried out on a $LiNi_{1/2}Mn_{1/2}O_2$ electrode after charging to 5 V (Figure S3). Based on the charged capacity being 268 mAh g^{-1}, the crystal lattice was found to contain only 9% of Li ions, assuming that the only reaction that took place was Li extraction. Only diffraction peaks belonging to the cubic lattice were observed in the XRD pattern of the charged electrode. The cubic lattice parameter was calculated and plotted against the charge capacity (Fig. 9). The cubic lattice parameter did not change in the composition range of $x > 0.5$ in $Li_{1-x}Ni_{1/2}Mn_{1/2}O_2$, although it decreased linearly in the composition range of $x \leq 0.5$.

Discussion

Identification of the crystal structure of low-temperature $LiNi_{1/2}Mn_{1/2}O_2$

First, we consider a layered LT-LNMO structure with cation disorder of Li and M (M = Ni and Mn) ions. The observed intensity ratio of (003) to (104) diffraction peaks for a layered structure with cation disorder, $I_{(003)}/I_{(104)} = 0.86$, shows that the cation disorder is less than

Fig. 8 Charge and discharge curves of Li/ $LiNi_{1/2}Mn_{1/2}O_2$ cells operated at 0.25 mA cm^{-2} in the voltage range of 2.5–4.7 V over the initial 5 cycles. Vertical dashed line indicates the theoretical capacity assuming that all Li ions are extracted from the material
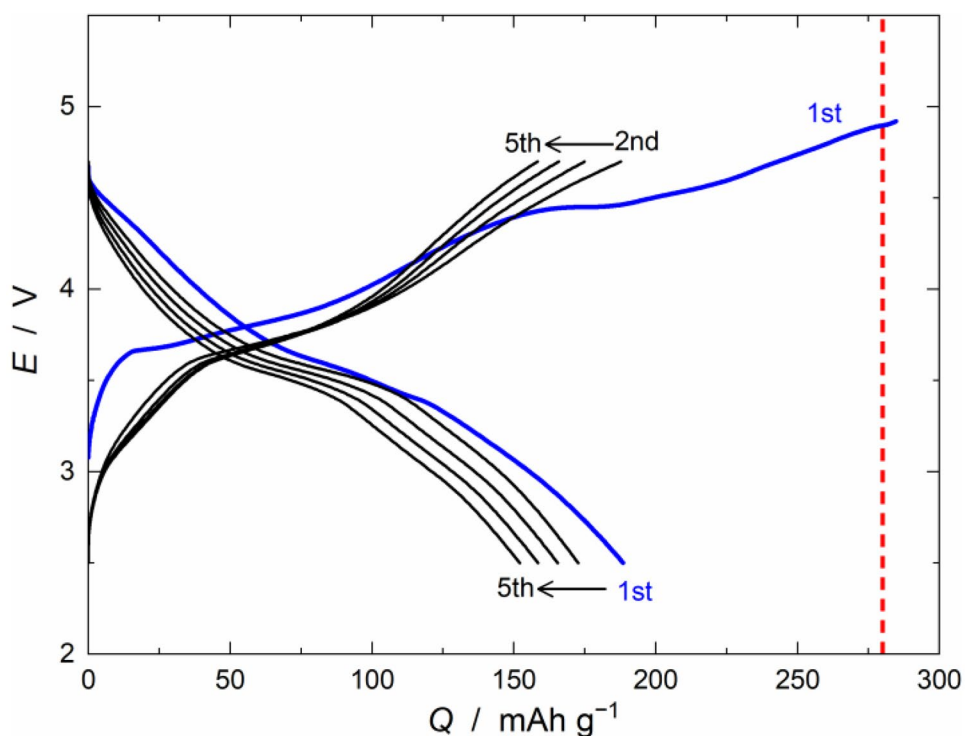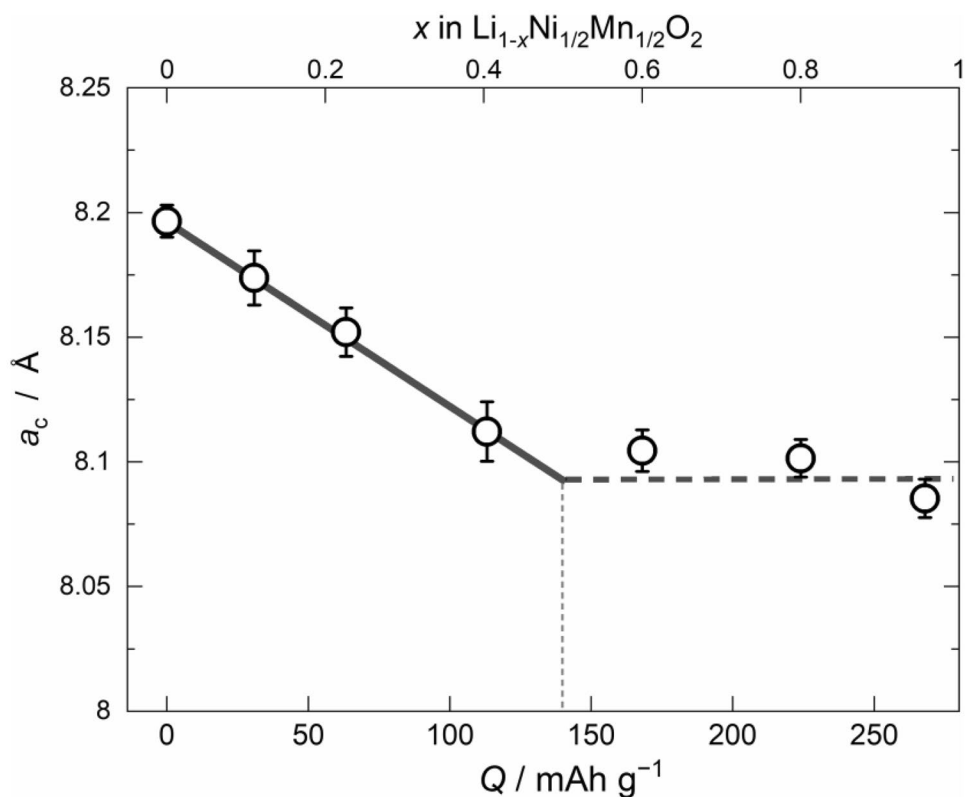
10% (Figure S4), which is too small to explain the isotropic lattice change during Li extraction from LT-LNMO. Moreover, the intensity ratio of LT-LNMO was similar to that of HT-LNMO, which has a layered structure $(I_{(003)}/I_{(104)} \sim 0.9)$ [40]. This is a clear evidence that the difference in the change in lattice parameter between LT and HT-LNMO during Li extraction is caused by the difference in the crystal structure, HT-LNMO has a two-dimensional framework, while LT-LNMO has a three-dimensional-framework.

Applying the extinction rule to its XRD pattern shows that LT-LNMO has a face-centered cubic structure. Therefore, LT-LNMO is limited to 11 possible space groups ($F23$, Fm-3, $F432$, etc.). Among these, all space groups except Fd-3, $F4_132$, Fd-3 m, and Fd-$3c$ have the reflection condition $h = 2n$ for ($h00$) reflections. Since the (200) reflection was not observed in the XRD pattern, LT-LNMO must belong to one of these space groups (Fd-3, $F4_132$, Fd-3 m, or Fd-$3c$). All cations in LT-LNMO occupy octahedral sites in a cubic-close packed oxygen arrangement, giving LT-LNMO a rock-salt structure. Therefore, the space group of LT-LNMO must be a subgroup of Fm-3 m to which the rock-salt structure belongs. The Fd-3 and $F4_132$ space groups can be excluded from consideration because these are subgroups of Fd-3 m. Two subgroups of Fd-3 m and Fd-$3c$ have a $2 \times 2 \times 2$ lattice indicative of Fm-3 m, which is in good agreement with the observation that the cubic lattice parameter of LT-LNMO

is twice that of the rock-salt structure. Reducing the space group symmetry from Fm-3 m to Fd-$3c$ provides one-to-one correspondence between the Wyckoff positions; 4a and 4b in Fm-3 m correspond to 32b and 32c in Fd-$3c$. Consequently, the locations of Li and M in the Fd-$3c$ space group cannot be distinguished in the crystal lattice (i.e., a random distribution of Li and M ions is observed). However, the space group of Fd-3 m enables the locations of Li and M to be distinguished because the Wycoff position of 4a in Fm-3 m is split into 16c and 16d in Fd-3 m, while 4b in Fm-3 m corresponds to 32e in Fd-3 m. Thus, the only possible space group to which LT-LNMO can belong is Fd-3 m. Therefore, LT-LNMO calcined at 500 °C is most likely to have the reduced spinel structure (space group: Fd-3 m), in which Li ions are located at the octahedral 16c sites, while Ni and Mn are randomly distributed throughout the octahedral 16d sites in a cubic close-packed oxygen array (32e sites).

The (400) peak is the strongest while the (111) peak is relatively weak in the XRD pattern of LT-LNMO (Fig. 5a), suggesting cation disorder of Li at the 16c sites and M at the 16d sites. Because the cation disorder results in the reduction of (111) peak intensity, however, hardly influences on (400) peak intensity, the degree of cation disorder can be estimated from the intensity ratio of the (111) and (400) peaks (Figure S5), where the intensities of (111) and (400) peaks of LT-LNMO were calculated using oxygen positional parameter, u, determined to be 0.255. Since the value of

u cannot be determined experimentally due to the broad diffraction peaks, we estimated *u* based on the ionic radii. When $u = 0.255$, Li–O and M–O bond lengths of 2.09 Å and 2.01 Å, respectively, were closest to the theoretical values of 2.16 Å and 2.01 Å calculated from the ionic radius [45]. From the observed intensity ratio (0.86), the cation disorder in LT-LNMO was approximately 8%, which is insufficient to prevent the Li extraction/insertion reaction.

Mechanism of the first lithium extraction/insertion cycle in $LiNi_{1/2}Mn_{1/2}O_2$

The change in the lattice constant shown in Fig. 7 verifies that 0.5 mol of Li ions was extracted from $LiNi_{1/2}Mn_{1/2}O_2$ in a topotactic manner. A cubic single-phase reaction mechanism was observed in LT-LNMO, in contrast to the cubic/tetragonal two-phase reaction observed in $LiMn_2O_4$ and $Li[Ni_{1/2}Mn_{3/2}]O_4$ [19, 43]. A significant difference between the voltage profiles of LT-LNMO and spinel materials was also observed, the profile of LT-LNMO was a sloping curve, while that of the spinel materials exhibited two voltage plateaus with a large voltage separation. This may be explained by the location of Li ions in $Li_{0.5}Ni_{1/2}Mn_{1/2}O_2$. If Li ions occupy half of the octahedral 16c sites without the formation of a spinel structure, the Li extraction reaction will proceed in a similar manner over the entire range, $0 < x < 1$ in $Li_{1-x}Ni_{1/2}Mn_{1/2}O_2$. At present, the crystal structure of $Li_{0.5}Ni_{1/2}Mn_{1/2}O_2$ is still unclear; thus, we are unable to fully explain the differences in the voltage profiles. Identifying the location of the Li ions in LT-LNMO during Li extraction is key to fully understanding the solid-state chemistry and electrochemistry of LT-LNMO, and this will be the focus of our future work.

There are two possible explanations for the change in the lattice dimensions observed in the high *Q* region of Fig. 9. The fact that the lattice constant does not change suggests that the electrolyte undergoes oxidative decomposition above 4.5 V. However, a highly reproducible charge capacity was observed (approximately 280 mAh g^{-1}, which is almost identical to the theoretical capacity), assuming that Li ions were completely extracted. Alternatively, Li extraction may proceed via a zero-strain reaction mechanism; however, a zero-strain reaction mechanism would be expected to induce a dimensional change owing to the oxidation of Ni^{3+} to Ni^{4+} during Li extraction [44]. Such a dimensional change has not been observed. In addition, no reduction peak corresponding to the oxidation peak at 4.45 V was observed in the differential chronopotentiogram (Figure S2), indicating that the reaction is irreversible in this voltage region. Although a discharge capacity of 180 mAh g^{-1} was measured, it is difficult to determine whether Li ions were extracted from $Li_{0.5}Ni_{1/2}Mn_{1/2}O_2$ because no change in the lattice dimension was observed. The lithium extraction mechanism of LT-LNMO thus remains unclear, and further investigation is required to elucidate the results presented herein.

Conclusion

In this study, it was found that $LiNi_{1/2}Mn_{1/2}O_2$ (LNMO) obtained by low-temperature (LT) synthesis has a cubic crystal lattice. This material is a polymorph of LNMO, which has a layered structure, obtained by high-temperature synthesis. As LNMO was synthesized at a LT, the c_h-axis contracted while the a_h-axis did not change. For the sample synthesized at ~ 500 °C, the c_h/a_h value, which represents crystal anisotropy, was 4.9 (i.e., that of a cubic lattice). Regardless of the synthesis temperature, LNMO was found to have a reversible capacity of approximately 120 mAh g^{-1}. With decreasing synthesis temperature, the charge–discharge curves changed to a gentler shape and the operating voltage decreased slightly.

Because the diffraction peaks of the sample prepared at a LT were too broad to determine the crystal lattice, the change in the lattice parameters during Li extraction was investigated. During Li extraction, both the a_h and c_h axes in the hexagonal lattice contracted, and the c_h/a_h ratio remained constant at approximately 4.9. This is clear evidence that LT-LNMO possesses a cubic lattice rather than a hexagonal lattice with pseudo-cubic lattice parameters. A plausible reduced spinel (or lithiated spinel) LT-LNMO structure in which Li and transition metal ions are regularly arranged in the octahedral sites of the cubic close-packed oxygen array was deduced by considering space group symmetry. The cubic lattice parameter was recalculated for the charged $LiNi_{1/2}Mn_{1/2}O_2$ and was found to change continuously from 8.20 Å for the pristine material to 8.11 Å for $Li_{0.6}Ni_{1/2}Mn_{1/2}O_2$, indicating that extraction of Li from $LiNi_{1/2}Mn_{1/2}O_2$ proceeds via a single-phase reaction.

When a charge–discharge test was conducted to examine the possibility of using $LiNi_{1/2}Mn_{1/2}O_2$ as a high-capacity positive electrode, the initial charge capacity was almost the same as the theoretical capacity, and the subsequent discharge capacity was 200 mAh g^{-1}. According to the XRD results, the cubic lattice parameter was almost constant for $Li_{1-x}Ni_{1/2}Mn_{1/2}O_2$ when $x > 0.5$. From these results, reduced spinel-structured $LiNi_{1/2}Mn_{1/2}O_2$ has the potential to be used as a high-capacity electrode material as it improves the reversibility of Li insertion/extraction.

By changing temperatures for syntheses, two polymorphs of $LiNi_{1/2}Mn_{1/2}O_2$ were obtained: one with a cubic lattice and the other with a hexagonal lattice. In these two polymorphs, although the solid-phase redox reaction was the same for Ni^{2+}/Ni^{4+}, their electrode potentials differed, as

did the change in their lattice dimensions during Li extraction. These differences clearly highlight the dependence of the mechanism by which lithium insertion occurs on the crystal structure. The detailed comparative examination of these presented in this study provides important information on the structural factors that affect lithium insertion.

Supplementary information The online version contains supplementary material available at https://doi.org/10.1007/s10008-021-05087-6.

References

1. Diouf B, Pode R (2015) Potential of lithium-ion batteries in renewable energy. Renew Energy 76:375–380
2. Manthiram A (2017) An outlook on lithium ion battery technology. ACS Cent Sci 3:1063–1069
3. Hesse HC, Schimpe M, Kucevic D, Jossen (2017) A Lithium-ion battery storage for the grid—a review of stationary battery storage system design tailored for applications in modern power grids. Energies 10:2107
4. Zubi G, Dufo-López R, Carvalho M, Pasaoglu G (2018) The lithium-ion battery: state of the art and future perspectives. Renew Sustain Energy Rev 89:292–308
5. Ohzuku T, Ueda A (1994) Why transition metal (di) oxides are the most attractive materials for batteries. Solid State Ion 69:201–211
6. Broussely M, Biensan P, Simon B (1999) Lithium insertion into host materials: the key to success for Li ion batteries. Electrochim Acta 45:3–22
7. Tarascon JM, Armand M (2001) Issues and challenges facing rechargeable lithium batteries. Nature 414:359–367
8. Goodenough JB, Park KS (2013) The Li-ion rechargeable battery: a perspective. J Am Chem Soc 135:1167–1176
9. Winter M, Besenhard JO, Spahr ME, Novák P (1998) Insertion electrode materials for rechargeable lithium batteries. Adv Mater 10:725–763
10. Delmas C, Ménétrier M, Croguennec L, Saadoune I, Rougier A, Pouillerie C, Prado G, Grüne M, Fournès L (1999) An overview of the Li(Ni, M)O$_2$ systems: syntheses, structures and properties. Electrochim Acta 45:243–253
11. Whittingham MS (2004) Lithium batteries and cathode materials. Chem Rev 104:4271–4301
12. Ohzuku T, Ariyoshi K, Makimura Y, Yabuuchi N, Sawai K (2005) Materials strategy for advanced lithium-ion (shuttlecock) batteries: lithium nickel manganese oxides with or without cobalt. Electrochemistry 73:2–11
13. Ellis BL, Lee KT, Nazar LF (2010) Positive electrode materials for Li-ion and Li-batteries. Chem Mater 22:691–714
14. Li W, Song B, Manthiram A (2017) High-voltage Positive electrode materials for lithium-ion batteries. Chem Soc Rev 46:3006–3059
15. Yano A, Shikano M, Ueda A, Sakaebe H, Ogumi Z (2017) LiCoO$_2$ Degradation behavior in the high-voltage phase transition region and improved reversibility with surface coating. J Electrochem Soc 164:A6116–A6122
16. Duffiet M, Blangero M, Cabelguen PE, Delmas C, Carlier D (2018) Influence of the initial Li/Co ratio in LiCoO$_2$ on the high-voltage phase-transitions mechanisms. J Phys Chem Lett 9:5334–5338
17. Hirooka M, Sekiya T, Omomo Y, Yamada M, Katayama H, Okumura T, Yamada Y, Ariyoshi K (2019) Degradation mechanism of LiCoO$_2$ under float charge conditions and high temperatures. Electrochim Acta 320:134596
18. Hirooka M, Sekiya T, Omomo Y, Yamada M, Katayama H, Okumura T, Yamada Y, Ariyoshi K (2020) Improvement of float charge durability for LiCoO$_2$ electrodes under high voltage and storage temperature by suppressing O1-phase transition. J Power Sources 463:228127
19. Ohzuku T, Kitagawa M, Hirai T (1990) Electrochemistry of manganese dioxide in lithium nonaqueous cell: III. X-ray diffractional study on the reduction of spinel-related manganese dioxide. J Electrochem Soc 137:769–775
20. Xia Y, Yoshio M (1996) An investigation of lithium ion insertion into spinel structure Li-Mn-O compounds. J Electrochem Soc 143:825–833
21. Kunduraci M, Amatucci GG (2006) Synthesis and characterization of nanostructured 4.7 V Li$_x$Mn$_{1.5}$Ni$_{0.5}$O$_4$ spinels for high-power lithium-ion batteries. J Electrochem Soc 153:A1345–A1352
22. Ariyoshi K, Yamamoto H, Yamada Y (2018) High dimensional stability of LiCoMnO$_4$ as positive electrodes operating at high voltage for lithium-ion batteries with a long cycle life. Electrochim Acta 260:498–503
23. Kim JS, Kim K, Cho W, Shin WH, Kanno R, Choi JW (2012) A truncated manganese spinel cathode for excellent power and lifetime in lithium-ion batteries. Nano Lett 12:6358–6365
24. Ariyoshi K. Eguchi. M, Hirooka M (2020) Examining the long-term cyclabilities of Li[Ni$_{1/2}$Mn$_{3/2}$]O$_4$ and Li[Li$_{0.1}$Al$_{0.1}$Mn$_{1.8}$]O$_4$ using a full-cell configuration including LTO-counter electrodes with extra capacity. J Electrochem Soc 167:060532
25. Huang Y, Dong Y, Li S, Lee J, Wang C, Zhu Z, Xue W, Li Y, Li J (2021) Lithium manganese spinel cathodes for lithium-ion batteries. Adv Energy Mater 11:2000997
26. Rossen E, Reimers JN, Dahn JR (1993) Synthesis and electrochemistry of spinel LT-LiCoO$_2$. Solid State Ionics 62:53–60
27. Shao-Horn Y, Hackney SA, Johnson CS, Kahaian AJ, Thackeray MM (1998) Structural features of low-temperature LiCoO$_2$ and acid-delithiated products. J Solid State Chem 140:116–127
28. Shao-Horn Y, Hackney SA, Kahaian AJ, Thackeray MM (2002) Structural stability of LiCoO$_2$ at 400 °C. J Solid State Chem 168:60–68
29. Antolini E (2004) LiCoO$_2$: Formation, structure, lithium and oxygen nonstoichiometry, electrochemical behaviour and transport properties. Solid State Ion 170:159–171
30. Lee E, Blauwkamp J, Castro FC, Wu J, Dravid VP, Yan P, Wang C, Kim S, Wolverton C, Benedek R, Dogan F, Park JS, Croy JR, Thackeray MM (2016) Exploring lithium–cobalt–nickel oxide spinel electrodes for ≥3.5 v Li-ion cells. ACS Appl Mater Interfaces 8:27720–27729
31. Ariyoshi K, Orikasa Y, Kajikawa K, Yamada Y (2019) Li$_2$Ni$_{0.2}$Co$_{1.8}$O$_4$ having a spinel framework as a zero-strain positive electrode material for lithium-ion batteries. J Mater Chem A 7:13641–13649
32. Lee E, Kwon BJ, Dogan F, Ren Y, Croy JR, Thackeray MM (2019) Lithiated spinel LiCo$_{1-x}$Al$_x$O$_2$ as a stable zero-strain cathode. ACS Appl Energy Mater 2:6170–6175
33. Ariyoshi K, Yuzawa K, Yamada Y (2020) Reaction mechanism and kinetic analysis of the solid-state reaction to synthesize single-phase Li$_2$Co$_2$O$_4$ spinel. J Phys Chem C 124:8170–8177

34. Ohzuku T, Ueda A (1994) Solid-state redox reactions of LiCoO$_2$ (R3m) for 4 volt secondary lithium cells. J Electrochem Soc 141:2972–2977

35. Lyu Y, Wu X, Wang K, Feng Z, Cheng T, Liu Y, Wang M, Chen R, Xu L, Zhou J, Lu Y, Guo B (2021) An overview on the advances of LiCoO$_2$ cathodes for lithium-ion batteries. Adv Energy Mater 11:2000982

36. Ohzuku T, Makimura Y (2001) Layered lithium insertion material of LiNi$_{1/2}$Mn$_{1/2}$O$_2$: a possible alternative to LiCoO$_2$ for advanced lithium-ion batteries. Chem Lett 30:744–745

37. Makimura Y, Ohzuku T (2003) Lithium insertion material of LiNi$_{1/2}$Mn$_{1/2}$O$_2$ for advanced lithium-ion batteries. J Power Sources 119–121:156–160

38. Meng YS, Ceder G, Grey CP, Shao-Horn Y-S, Y, (2004) Understanding the crystal structure of layered LiNi$_{0.5}$Mn$_{0.5}$O$_2$ by electron diffraction and powder diffraction simulation. Electrochem Solid-State Lett 7:A155–A158

39. Bréger J, Meng YS, Hinuma Y, Kumar S, Kang K, Shao-Horn Y, Ceder G, Grey CP (2006) Effect of electron diffraction and powder diffraction simulation of LiNi$_{0.5}$Mn$_{0.5}$O$_2$: a joint experimental and theoretical study. Chem Mater 18:4768–4781

40. Ariyoshi K, Ichikawa T, Ohzuku T (2008) Structural change of LiNi$_{1/2}$Mn$_{1/2}$O$_2$ during charge and discharge in nonaqueous lithium cells. J Phys Chem Solids 69:1238–1241

41. Gummow RJ, Liles DC, Thackeray MM (1993) Spinel versus layered structures for lithium cobalt oxide synthesised at 400 °C. Mater Res Bull 28:235–246

42. Gummow RJ, Liles DC, Thackeray MM, David WIF (1993) A reinvestigation of the structures of lithium-cobalt-oxides with neutron-diffraction data. Mater Res Bull 28:1177–1184

43. Ariyoshi K, Iwakoshi Y, Nakayama N, Ohzuku T (2004) Topotactic two-phase reactions of Li[Ni$_{1/2}$Mn$_{3/2}$]O$_4$ (P4$_3$32) in nonaqueous lithium cells. J Electrochem Soc 151:A296–A303

44. Ariyoshi K, Yamamoto H, Yamada Y (2019) Relationship between changes in ionic radius and lattice dimension of lithium manganese oxide spinels during lithium insertion/extraction. Solid State Ion 343:115077

45. Shannon RD (1976) Revised effective ionic radii and systematic studies of interatomic distances in halides and chalcogenides. Acta Crystall A 32:751–767